Int J Adv Manuf Technol (2014) 75:373–384
DOI 10.1007/s00170-014-6158-z

ORIGINAL ARTICLE

Material characterizations of mild steels, stainless steels, and both steel mixed joints under resistance spot welding (2-mm sheets)

Nachimani Charde · Farazila Yusof · Rajprasad Rajkumar

Received: 13 March 2014 / Accepted: 7 July 2014 / Published online: 19 July 2014

Abstract Resistance spot welding is an essential welding mechanism for joining two or more metal sheets together in automotive industries. The mechanical assemblies are easily joined at discrete spots using high current flow through the area of concentration. It is easily achieved by compressing the base metals together to a certain pressure using copper electrode caps and allow the high current to flow through the concerned areas. The heat generation due to the current flow causes the metal sheets to be fused and consequently form bonds between base metals. The molten areas of base metals undergo solidification process by itself when the current flow is utterly stopped. Basically, the weld growth in any joint is determined by its process-controlling parameters, particularly the welding current, weld time, electrode force, and electrode tip. In these experiments, the welding current and weld time variations were carried out to characterize the weld growth for three types of joints mainly for stainless steel, mild steel, and both steel mixed joint. A pneumatically driven 75-kVA spot welder was used to accomplish the entire welding processes, and the welded samples were later subjected to tensile, hardness, and metallurgical tests to relate the diameter growth, loading force during tensile test, failure crack initiation, post-failure crack propagation direction, macro and microstructural changes, and also the hardness changes due to solidification process. Assessing the experimental results of 2-mm thickness of materials revealed that the welded areas' characteristics have been varied from its original states to enriched states, in terms of shearing strength and hardness distribution as well as the microstructural orientation.

Keyword Stainless steel welding · Mild steel welding · Joined materials · Dissimilar joints

N. Charde (✉) · F. Yusof
Department of Engineering Design and Manufacture, Faculty of Engineering, University of Malaya, 50603 Kuala Lumpur, Malaysia
e-mail: Nachi.charde@nottingham.edu.my

F. Yusof
e-mail: farazila@um.edu.my

R. Rajkumar
Department of Mechanical, Material and Manufacturing Engineering, The University of Nottingham UK, Malaysia Campus, JalanBroga, 43500 Semenyih, Selangor Darul Ehsan, Malaysia
e-mail: rajprasad.rajkumar@nottingham.edu.my

1 Introduction

A common metal-joining technique that used to join two or more metal sheets together through fusion is called as spot welding. It is accomplished by allowing high current to flow through metal sheets at discrete spots. The welding current and weld time lead the root penetration between metals while the electrode pressing force and electrode tips hold the spots firmly in a welding process [1]. This process basically uses two copper electrodes to compress the sheets together and supplies huge amount of current (typically kA) through the contact area of electrodes. The flow of welding current against the series of resistances (electrodes to sheets' resistances, bulk resistances, and sheets to sheets' resistances) establish resistive path for high current flow. These huge amounts of current flow cause heat generation and gradually melt the faying surfaces of base metals as the time goes during the welding process [2, 3]. The highest resistive areas will initially be melted, and the melt itself grows or expands in all direction equally for similar base metals. As for the dissimilar weld joints, there will be heat imbalance occurrences in the weld geometry resulting in different weld diameters [4]. Once the current flow is fully stopped, the fused area will then be solidified. The diameter growth of solidified areas between mild steel and stainless steel varies from each other as mild steels offer its critical diameter growth as $3t^{0.5}$ whereas the

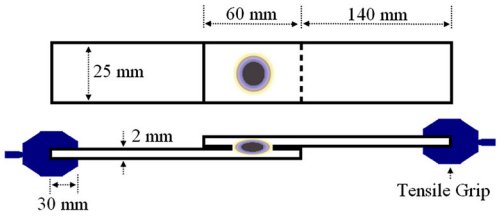

Fig. 1 Test sample

stainless steels offer its critical diameter growth as $4t^{0.5}$; let '*t*' be the thickness of base metals in millimeter [5, 6]. The fused and solidified areas of base metals are called as weld nuggets from here on and it consists of four major zones. They are categorized as fusion zone (FZ) or weld nugget, heat-affected zone (HAZ), heat-extended zones (HEZ), and base metals (BM). Some researchers combine the heat-affected and heat-extended zones as one region, but I treat it separately so as to compare with SORPAS simulation results. The proper weld joints or bonds between sheets are usually formed by the fusion zones at which the microstructural alterations fully happened during solidification. The heat-affected zones do exist due to the thermal conduction around the fusion zones and also altered the microstructures partially. However, the heat-extended zone does exist because of the materials' thermal conductivity rates. This region is still categorized under the heat-affected zones because of the partial or sometime minimal microstructural changes. These regions are certainly seen in mild steel as compared to stainless steel in addition to the dissimilar weld joint. The other part of the entire base metals remained unchanged. The weld nugget growths are basically determined by the controlling parameters, primarily the welding current, welding time, electrode pressing force, and electrode tip diameter [7]. These are the four common parameters that enable a weld growth as it influences sound welds to prolong the stiffness of any metal joints. In this experiment, the current and weld time were varied while

Table 1 Chemical and mechanical properties of base metals

304 austenitic stainless steel and mild steel		
Element	Weight %	Weight %
C	0.046	0.23
Cr	18.14	
Ni	8.13	
Mn	1.205	0.095
Si	0.506	0.006
S	0.004	0.050
N	0.051	
P	0.030	0.040
Hardness (HRB)	86.2	65

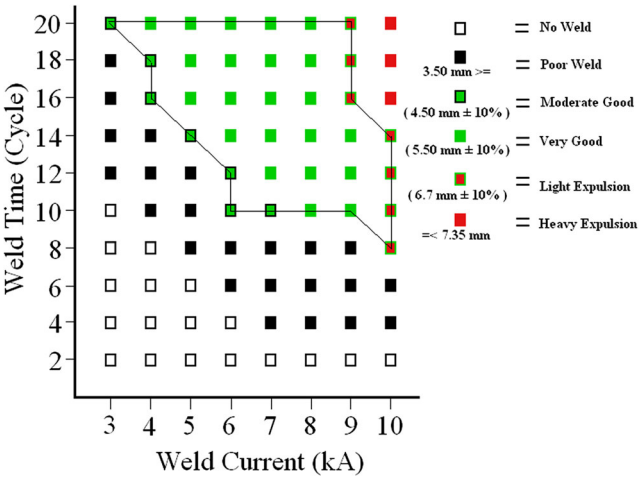

Fig. 2 Welding lobe diagram

electrode force and tips remained unchanged to characterize the weld growth for 2-mm base metals of stainless steel and mild steel sheets as 2-mm thickness is very rare in size that is used in spot-welding research. As such, this paper will lead to new understanding of higher-thickness materials in RSW.

2 Experimental

The specimens were prepared in rectangular shape metal sheets (200 mm×25 mm×2 mm) as shown in Fig. 1, and its chemical and mechanical properties are listed in Table 1. A pair of water-cooled copper electrodes with truncated tip diameters of 5 mm was used to join these metal sheets which were selected from RWMA's class two (copper and chromium) category. Two separate specimens were initially placed on the top of the lower electrode tip of the spot welder (AC waveform, 75 kVA) as overlaying 60 mm on each other and then the initiating pedal was pressed to squeeze the middle of 60-mm overlap. The welding process was started immediately after the electrode pressing force reached its present value of preset force. The welding current flow falls in kilo ampere ranges as sinusoidal waveform, and the repetition of waveform is counted as weld cycles. So the welding current flow was lasted for the given weld time. Thereafter, the pneumatic-driven electrodes' pressing mechanism consumes some time for cold work (for the solidification process) and finally return back to the home position of the electrode assembly. The welding process controlling parameters (current, weld time, and force) are set before the welding process starts so that the weldment happens in accordance with the preset values. Meanwhile, the squeeze cycle was 35, hold cycle was 20, and cooling cycle was 20 in the welding sequence.

However, in order to estimate the reasonable working region to avoid the expulsion and poor weld conditions, some

Table 2 Weld schedule for process-controlling parameter

Sample no.	Weld schedule	Material	Electrode tip (mm)	Force (kN)	Current (kA)	Time (cycle)
1–7	1	MS, SS & MS + SS	5	3	7	10
8–14	2	MS, SS & MS + SS	5	3	8	10
15–21	3	MS, SS & MS + SS	5	3	9	10
22–28	4	MS, SS & MS + SS	5	3	7	15
28–35	5	MS, SS & MS + SS	5	3	8	15
36–42	6	MS, SS & MS + SS	5	3	9	15
43–49	7	MS, SS & MS + SS	5	3	7	20
50–56	8	MS, SS & MS + SS	5	3	8	20
57–63	9	MS, SS & MS + SS	5	3	9	20

welding processes were conducted prior to final experiments. By done so, the good working region was predicted, and the result is shown in Fig. 2.

Figure 2 shows the welding lobe curve for 2-mm sample sheets with constant force (3 kN) and unchanged circle electrode tips (5 mm of diameter). The electrode force and electrode tip were selected based on the manufacturers' manual. Thus, according to Fig. 2, the weld lobe boundary indicated by continuous black color lines delineates all acceptable welding regions. The colored symbols represent the quality of welds that produced, and conditions that did not produce any weld are indicated by white boxes. The green-colored boxes with black borders represent moderate to good welds; the fully green boxes represent very good welds; the red-colored boxes bordered in green represent welds for which light expulsion occurred; the red boxes represent heavy expulsion; and the black boxes represent poor weld joints. A weld schedule was initially developed based on the welding lobe to avoid expulsion and poor welding conditions because the scope of this paper is to investigate the weld growth in good working regions. So the process parameters that of the welding current and welding time are equally spaced between their regions. Assumption follows the welding lobe contour and therefore three levels of welding current (7, 8, 9 kA) and welding time (10, 15, 20 cycle) were established. Based on this simple prediction, nine weld schedules were finalized as listed in Table 2. During the welding process, seven pairs of base metals were developed for each weld schedule. Five out of seven were used for tensile test, and the corresponding average value was considered for that particular weld schedule. One pair of specimen was used for hardness test, and the final one pair of specimen was used for metallurgical test.

The tensile shear test was carried out using 100 kN tensile testing machine to determine strength of welded samples. The crosshead speed was maintained at 70 mm/min, and the metal sheets were held for 30-mm tensile grip out of 200-mm original length as shown in Fig. 1. The ultimate tensile strength (UTS) was measured as the maximum weld strength after which the welded sample will crack itself (Fig. 3). An average strength value of the five samples for each weld schedule was taken as final values of that particular weld schedule [8].

The hardness test was carried out using a Rockwell hardness tester applying scale 'B' with 20 kg of pressing force. Twenty two points were measured from the left hand side of base metal through the welded areas and ended at the right hand side of base metal. Figure 4 shows the hardness measuring point of a dissimilar welded joint. The test was conducted

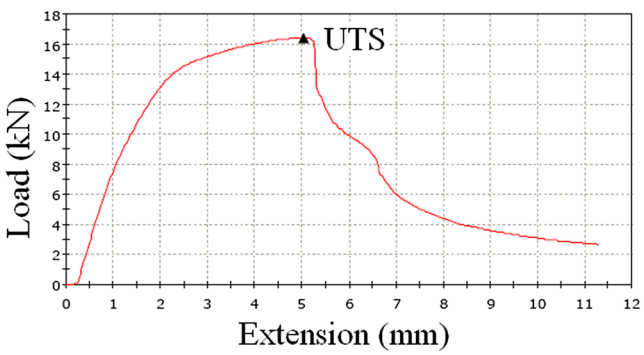

Fig. 3 Tensile shear test (ultimate tensile strength)

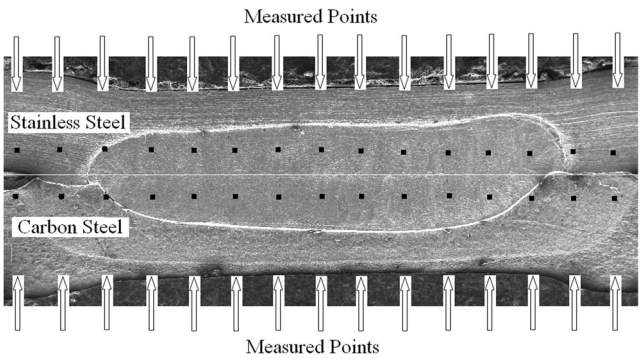

Fig. 4 Hardness test using Rockwell hardness machine (scale B)

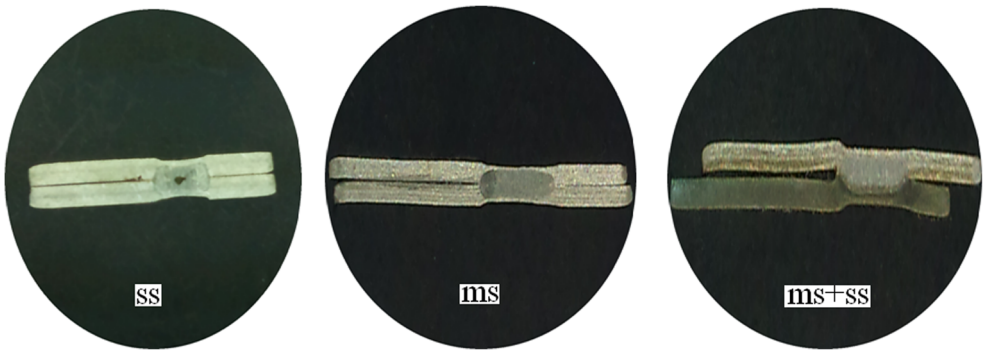

Fig. 5 Samples that mounted on resin power

Table 3 General properties of base metals

Properties	Stainless steel	Mild steel
Density	8.00 g/cm^3	7.85 g/cm^3
Melting point	1,400–1,450 °C	1,426–1,538 °C
Electrical resistivity	$6.89\times10^{-7}\Omega$.m	$1.611\times10^{-7}\Omega$.m
Thermal conductivity	16.2 W/m.K (min)	54 W/m.K (min)
Thermal expansion	17.2×10^{-6}/K	12×10^{-6}/K

for both sides of welded joint. However, for the mild steel and stainless steels, only one side of measurement was taken into consideration though both sides were measured.

The welded samples for the mild, stainless, and mixed steel were cut at the line of its diameter and mounted it using resin powder on hot press mount machine. The mounted samples (Fig. 5) were roughly polished using silicon papers 1,200/800 p and 600/200 p and also continuously further polished

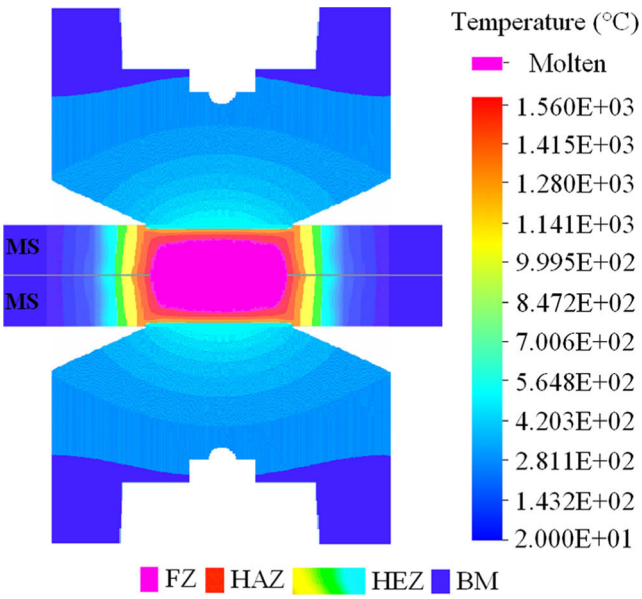

Fig. 6 A simulation work for 8 kA, 15 cycles, and 3 kN of force (2-mm mild steel)

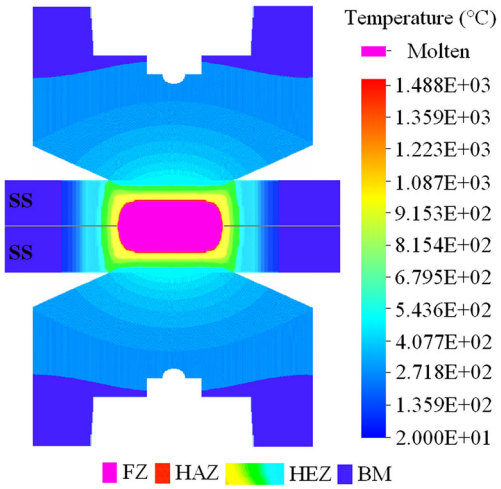

Fig. 7 A simulation work for 8 kA, 15 cycles, and 3 kN of force (2-mm stainless steel)

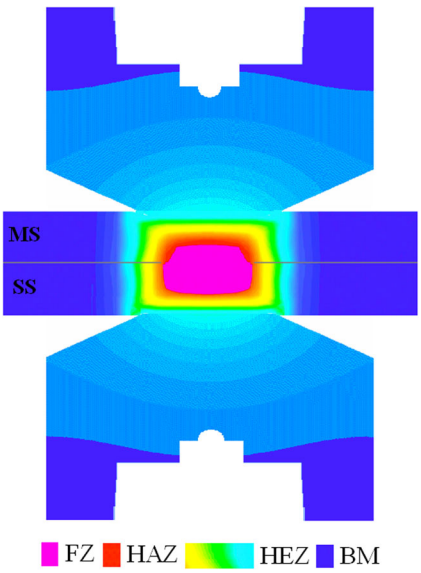

Fig. 8 A simulation work for 8 kA, 15 cycles, and 3 kN of force (2-mm mild and stainless steel)

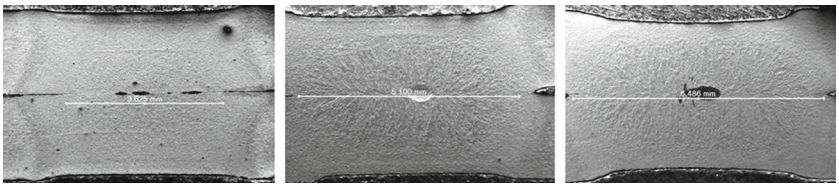

a) 10 Cycle b) 15 Cycle c) 20 Cycle

Fig. 9 Diameter increment of mild steel (weld time increment). **a** 10 cycles, **b** 15 cycles, **c** 20 cycles

using Metadi polishing cloth with suspension liquid of 0.05 micron. This polishing process has been conducted for about 30 min to 1 h on each sample until the shining surfaces were seen. The well-polished samples were later kept in nitrogen-filled chamber to reduce the oxidation effects before taking into the SEM scanner. At last, the ferric chloride (500 ml for 10 samples) was used to etch these well-prepared samples in a pot for about 30–45 min. After that, the samples were rinsed off using plain water and dried using an air blower. It was sent to SEM scanning procedures without any delay because the mild steels are very sensitive to atmospheric moisture.

3 Results and discussion

3.1 A comparative study of simulation and real weld joints

Simulation procedures for the similar and dissimilar weld joints (mild and stainless steel) were performed using SORPAS, the spot-welding process software before the real experiment starts. In SORPAS, the electrical-mechanical-thermal characteristics' equations or boundary conditions or contact resistance's characteristics are all built in so the user has to select only few parameters such as the thickness of base metals, material type, electrode tip diameter, process parameters, and so on. As the results of simulation works for mild, stainless, and mixed steels, symmetrical weld zones for similar steels and asymmetrical weld zones for dissimilar steels were obtained. These are quite possible because of the different electrical properties of base materials which may lead to different thermal flow characteristics (Table 3). Thereby, the simulative results of welded zones are categorized into four regions so as to compare with the real welded samples precisely. The noticeable zones are firstly, the fusion zone, secondly, the heat-affected zone, thirdly, the heat-extended zone, and fourthly, the base metal.

Table 3 lists the general properties of mild and stainless steels. From the table itself, it is clearly seen that the melting point of both materials are slightly differed from each other so the melting process starts at different rates of temperature when fused together.

As for the mild steel weld joint (Fig. 6), it is simulated for 8 kA, 15 cycles, and 3 kN of force. The thermal conductivity rate is higher as compared to stainless steels and therefore wider range of heat-affected (HAZ) and heat-extended (HEZ) zones is noticed in the mild steel welds [9]. However, the fusion zone of mild steel seemed to be shorter in diameter as compared to stainless steel because of the thermal expansion rate. It can be compared from the simulation results for both steels (Fig. 7).

On the other hand, the thermal conductivity rate is lower in stainless steel as compared to mild steel which results in shorter heat-affected and heat-extended regions. However, the diameter of welded regions looked to be wider as compared to mild steel due to the thermal expansion rate [10]. This phenomenon is certainly noticed when both sheets were welded together. Figure 8 shows the asymmetrical weld regions as it contained dissimilar metal sheets of mild and stainless steels [11]. So it is now clearly seen that the welded areas in dissimilar steels have heat imbalances and resulting asymmetrical weld bead.

3.2 Diameter increments and tensile shear test

The diameters' increment and the tensile shear forces are directly related to each other. When the welding current and weld time are increased according to the welding lobe's limit, the weld nuggets' diameters are also increased correspondingly. The diameter increments cause stronger bonds between

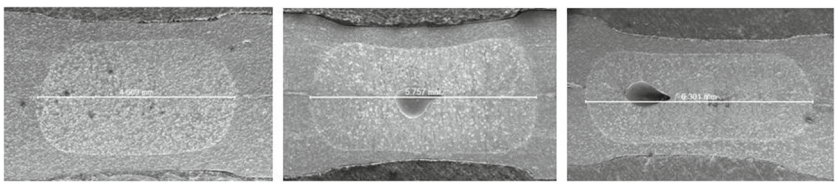

a) 10 Cycle b) 15 Cycle c) 20 Cycle

Fig. 10 Diameter increment of stainless steel (weld time increment). **a** 10 cycles. **b** 15 cycles. **c** 20 cycles

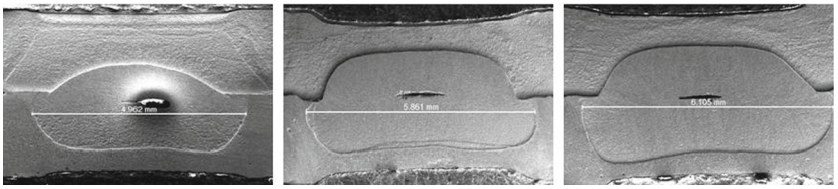

a) 10 Cycle b) 15 Cycle c) 20 Cycle

Fig. 11 Diameter increment of dissimilar (mild + stainless) steel (weld time increment). **a** 10 cycles. **b** 15 cycles. **c** 20 cycles

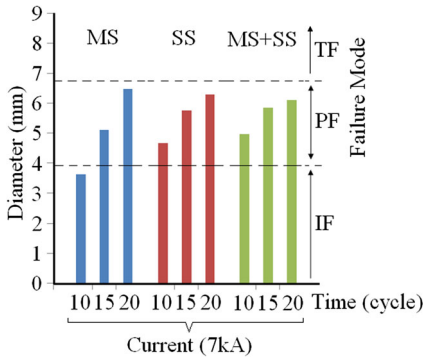

Fig. 12 Diameter increment for all the material (weld time increments)

sheets and therefore more tensile shear force is required to break the weld joints. Figures 9, 10, and 11 are showing the samples that subjected to weld time increments. A comparison of all the three different weld joints and the corresponding tensile failure modes is shown in Fig. 12 for the weld time increments.

Similarly, Figs. 13, 14, and 15 are showing the samples that subjected to welding current increments. A comparison of all the three different weld joints and the corresponding tensile failure modes are shown in Fig. 16 for the welding current increments.

Having considered the tensile shear test, the welding current and weld time increments have proportionally increased the diameters of welded areas and required more tensile shear forces to break the bonds between metal sheets (weld joints) regardless of base metals [12]. For instance, when the current from 7 to 8 kA and 8 to 9 kA were increased, the diameters of weld nuggets were increased and consequently more tensile force were drawn to break the welded joints. Similar type of tensile force increments was noticed for the weld time increments. Thus, when the weld time from 10 to 15 cycles and 15 to 20 cycles were gradually increased, the diameters of weld nuggets increased and thereby higher tensile forces were required to break the bounds as how we saw in the welding current increments. It may be recalled from the Joules law to understand mathematically that the heat is proportional to the squared welding current and the resistance of the path as well as the welding time ($Q=I^2Rt$). Moreover, the tensile shear force of stainless steel seemed to be higher as compared to mild steel because of the natural material strength. However, the mixed steels' strength fall between both steels' strength as shown in Fig. 3. The tensile test results are shown in Fig. 3 for mild steel, stainless steel, and both steel mixed joints (Fig. 17).

3.3 Failure modes of tensile test

Having considered the failure modes of tensile test, the conventional way of checking the crack initiations is followed in accordance with weld types. For example, an improper or insufficient weld joint will fracture itself as interfacial failure and a better weld joint will fracture itself as pullout fracture [13, 14]. By checking so, there is no difference between better and best weld joint, although it can be used to differentiate from poor failures (IF). Hence, the post-crack initiating propagation was observed in this experiment in order to differentiate the better and best weld joints. In such ways, the interfacial fracture (IF) is still remained as interfacial failure (IF) but the pullout failure is divided into two category as partial fracture (PF) and pullout fracture or button pullout (TF). Thus, a moderately good weld has crack from heat-affected zone of either sides and the resulting partial fracture (PF) of base metals. These types of fractures are acceptable as good weld joints, but it has high tendency of neck breaking during tensile test. However, a very good weld has better bonding between sheets and resulting tear from both sides (TF) when post-crack

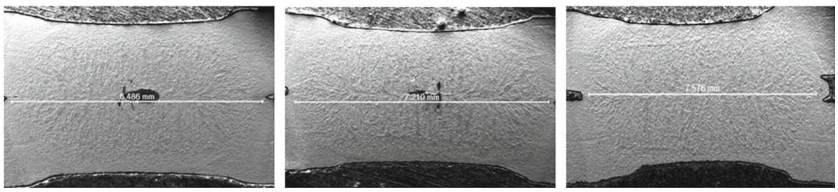

a) 7 kA b) 8 kA c) 9 kA

Fig. 13 Diameter increment of mild steel (welding current increments).**a** 7 kA, **b** 8 kA, **c** 9 kA

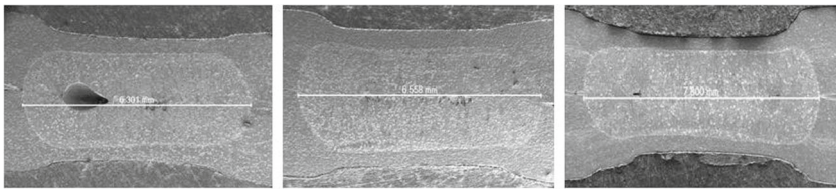

Fig. 14 Diameter increment of stainless steel (welding current increments). **a** 7 kA, **b** 8 kA, **c** 9 kA

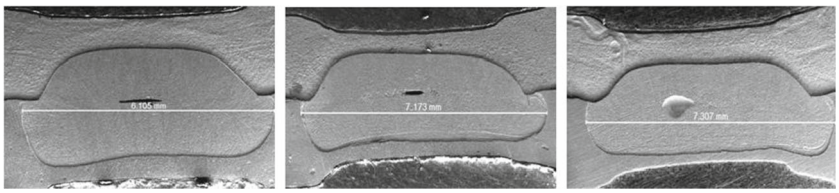

Fig. 15 Diameter increment of dissimilar (mild + stainless) steel (welding current increments). **a** 7 kA, **b** 8 kA, **c** 9 kA

failure test is carried out. So the post-crack-initiating propagation was studied to differentiate the better and best weld joints. Furthermore, when dissimilar weld joints are subjected to tensile shear test, the weaker side (mild steel) breaks first and consecutively the stronger side (stainless steel) follows thereafter. In this experiment, the post-crack failures are noticed for all the three different weld joints. Figure 18a shows the exact places where the crack initiates during tensile test, and the following figures (Fig. 18b–d) are showing the mild steels, stainless steels, and both steels' mixed post-crack failures, respectively.

3.4 Metallurgical study

The metallurgical study of mild, stainless, and mixed steels' weld joints have given clear pictures of weld nugget diameters and its microstructural organizations. The fusion zone of mild steel seemed to be coarse grains while the heat-affected areas seemed to be finer grains regardless of controlling parameter changes. The macro and micrographs of these patterns have been noticed for mild steel and it has been shown in Fig. 19a–d.

The parameter changes have directly influenced the grains at both: the fusion zones and the heat-affected zones. The base metals' microstructures have more pearlite and less ferrite in its region as how it was made about with smaller grains as compared to the other two zones. The heat-affected zones are transformed into martensite phases with some areas of pearlite and ferrite with refined grains. Moreover, the heat-extended zones are also slightly affected with this transformation. However, the fusion zones seemed to be coarsened and were larger in grain size as compared to the other two regions. This region had the highest martensite formation with very few areas of pearlite nodules [15]. Similar types of results were noticed for austenitic stainless steel except the heat-affected zones. The heat-affected zones were seen to be a much narrowed region next to the fusion zones, and the heat-extended zones are not completely seen [16]. Figure 20 shows the complete microstructure view of welded and unwelded areas of 2-mm austenitic stainless steel. The chromium (Cr) to nickel (Ni) ratio was altered during the welding process which resulted the lathy ferrite to be increased when it undergoes the cold work. During the solidification process, it transforms into austenite, leaving the core of ferritic dendrite as skeleton (vermicular) [17]. The columnar dendrites were rearranged randomly.

The heat imbalance (asymmetrical welded zone) is clearly seen in Fig. 21 as the mild and stainless steels have different thermal and electrical properties as seen in the simulation works [18]. The heat misbalancing problem can be overcome by using servo-based force actuator or using additional resistance pad between the electrode and stainless steel side as how American Welding Society suggests. Recalling the literature, the thermal conductivity coefficients (54 W/m.K (min)) are higher in mild steels as compared to stainless steels (16.2 W/m.K (min)); therefore, wider ranges of heat-affected zones (HAZ) are noticed. However, the thermal expansion

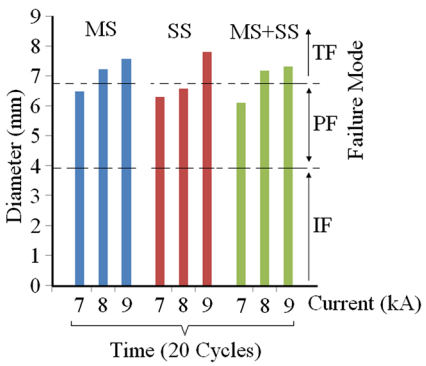

Fig. 16 Diameter increment for all the material (welding current increments)

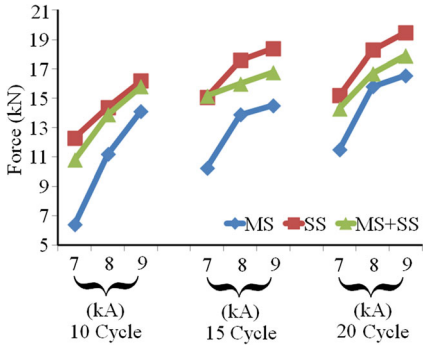

Fig. 17 Tensile test results

coefficient (12×10^{-6}/K) rate is lower which allows the thermal flow in the base metals so that the width and height of fusion zone is shorter in this side. On the other side, the stainless steel seemed to have higher thermal expansion coefficient (17.2×10^{-6}/K) but lower thermal conductivity. So the heat-affected zones (HAZ) are smaller, but the fusion zone is wider as compared to mild steels. Technically, this phenomenon is called as heat imbalance, and it can be overcome by using different types of electrode tips during welding.

3.5 Hardness test results

The hardness test was carried out for the mild steel, stainless steel, and both steel mixed weld [15–17]. The hardness was measured from left hand sides through the heat-affected zones then fusion zones then heat-affected zones again and ended up with the right hand side of base metals. The welded areas seemed to be increased in terms of hardness but vary from one material to another. Thus, when the mild steel is concerned, then the unwelded areas (BM) seemed to have an average hardness of 65 (HRB) but the welded areas seemed to be about 115 (HRB). This is very obvious that the hardness is almost

Fig. 18 **a** Crack-initiating points of failure modes. **b** Post-crack propagation mode of mild steel. **c** Post-crack propagation mode of stainless steel. **d** Post crack propagation mode of mild and stainless steel

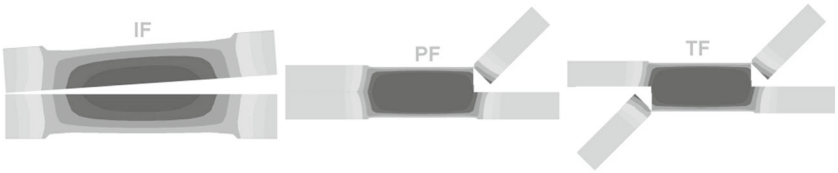

(a) Crack initiating points of failure modes

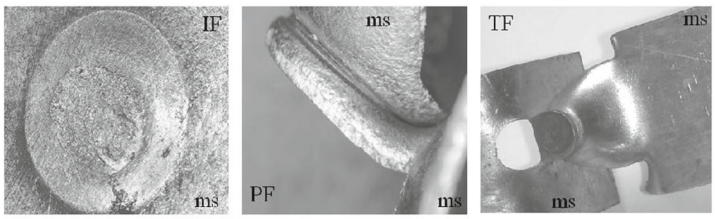

(b) Post crack propagation mode of mild steel

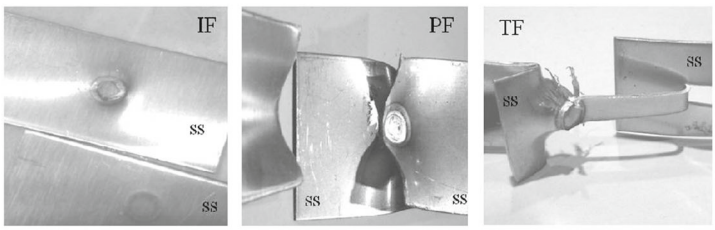

(c) Post crack propagation mode of stainless steel

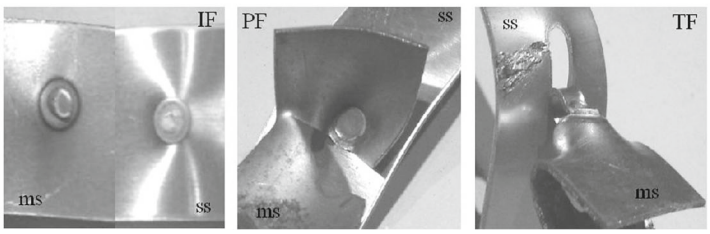

(d) Post crack propagation mode of mild and stainless steel

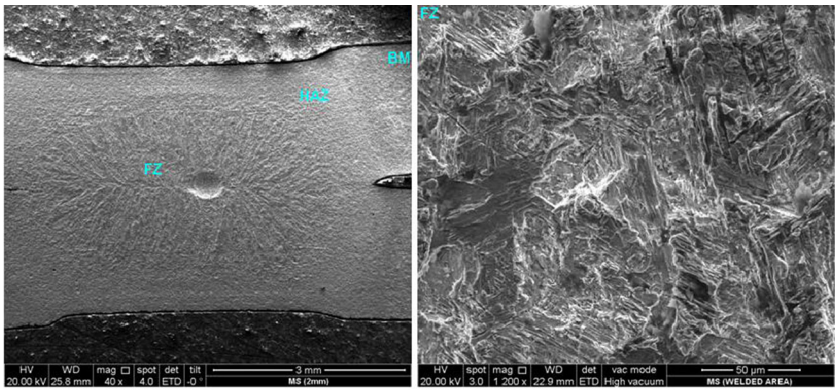

a) Macrograph of mild steel weldt b) Fusion zone of mild steel

c) Original micro structure of mild steel d) Heat affected zone of mild steel

Fig. 19 Microstructural view of mild steel (2 mm). **a** Macrograph of mild steel weld. **b** Fusion zone of mild steel. **c** Original microstructure of mild steel. **d** Heat-affected zone of mild steel

doubled in the mild steel when it solidifies. However, the hardness of heat-affected zones (HAZ) (95 HRB) is lower than the fusion zones but higher than the base metals (BM). Figure 22 shows the hardness distribution of mild steel.

Similar pattern of hardness distribution was seen for the stainless steels and mixed steel joints. However, the hardness of base metals of stainless steel seemed to be higher as compared to mild steel due to the nature of the material [18, 19]. It has an unwelded hardness of 86 (HRB), and the welded zones seemed to be around 96 (HRB). The heat-affected zones (HAZ) (90 HRB) are lower than the fusion zones (FZ) but slightly higher than base metals (BM). As for the mixed steel joints, the hardness is almost the same as mild steels for both sides (115 HRB). The hardness distributions at the fusion zones of all the base metals were fluctuated and create no relationship between one another for nine weld schedules no matter what the diameters are. It should be clearly noted here that the increment of current or weld time has no influence on the hardness distribution because the hardness changes happened in the mean of solidifications [20]. Figures 23 and 24 show the stainless steels and mixed steels' hardness distributions, respectively.

4 Conclusion

The mild and stainless steel (2-mm thickness) are reasonably welded with 3 kN of electrode pressing force; 5 mm of electrode cap diameter; 10, 15, and 20 weld cycles of time; 7, 8, and 9 kA of welding current in 75-kVA spot welder. It concludes that

(a) Simulation works are obviously showing the fusion zones (FZ), heat-affected zones (HAZ), heat-extended zones (HEZ), and base metals regardless of base metals.
(b) Increase in the welding current and welding time within the welding lobe has resulted an increment in the diameter of weld nuggets and therefore the increment of tensile shear force was noticed regardless of materials.
(c) Stainless steels have higher tensile shear forces as compared to mild steel welds and mixed welds due to the natural hardness of the material.
(d) The tensile shear forces (UTS) of mixed welds have fluctuated between the mild and stainless steels' shear forces.
(e) The common two failure modes were seen for crack initiation for all the weld joints as poor weld produces interfacial fracture (IF) and good weld produces button pullout or tear from both sides (TF).

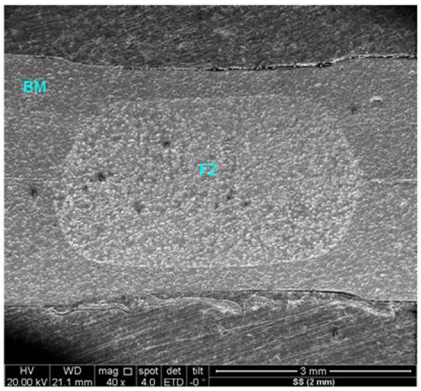

a) Macrograph of stainless steel weld

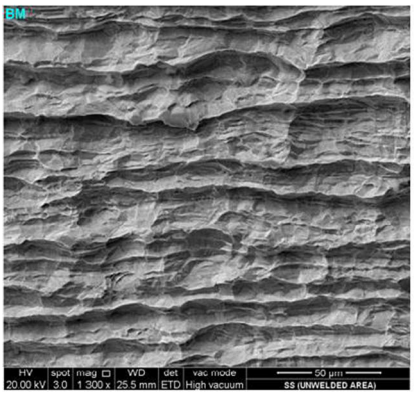

c) Original micro structure of stainless steel

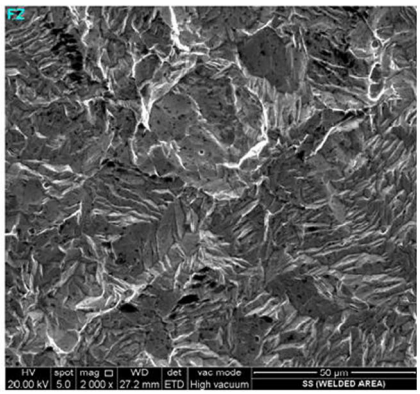

b) Fusion zone of stainless steel

Fig. 20 Microstructural view of stainless steel (2 mm). **a** Macrograph of stainless steel weld. **b** Fusion zone of stainless steel. **c** Original microstructure of stainless steel

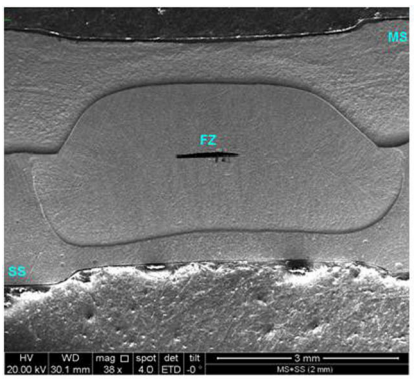

a) Macrograph of mixed steel weld

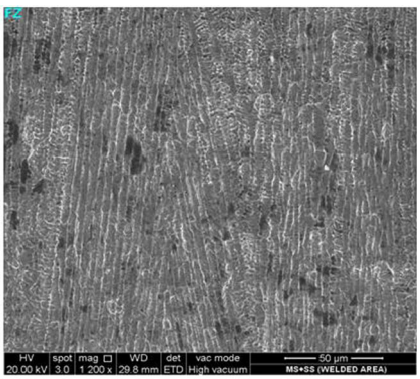

b) Fusion zone of mixed steel

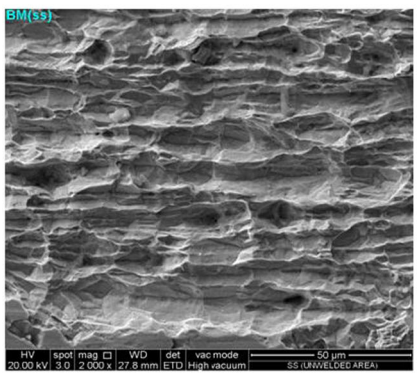

c) Original micro structure of stainless steel

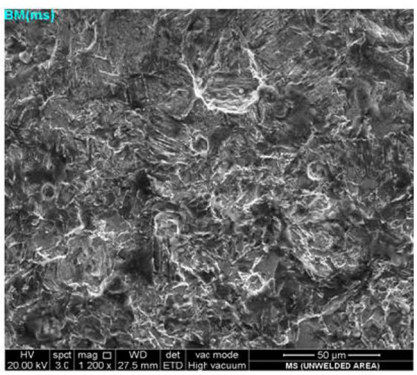

d) Original microstructure of mild steel

Fig. 21 Microstructural view of stainless steel and mild steel (2 mm). **a** Macrograph of mixed steel weld. **b** Fusion zone of mixed steel. **c** Original microstructure of stainless steel. **d** Original microstructure of mild steel

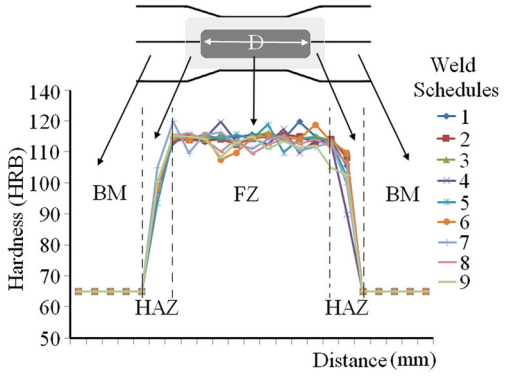

Fig. 22 Hardness of mild steel

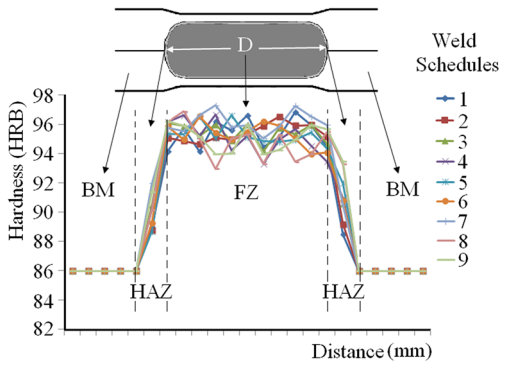

Fig. 23 Hardness of stainless steel

(f) Post-crack-initiating propagation was observed for all the weld joints and found that pullout failure mode (TF) was the best weld joint as compared to partial failure mode (PF) and interfacial failure mode (IF).

(g) Hardness of welded zones was increased to almost double the value for the mild and mixed steels. However, the hardness distribution across the fusion zone was fluctuated regardless of process parameter increments.

(h) Hardness of the stainless steels was slightly increased during solidification, but the distribution along the welded zones was fluctuating in values as how the mild and mixed steels have resulted.

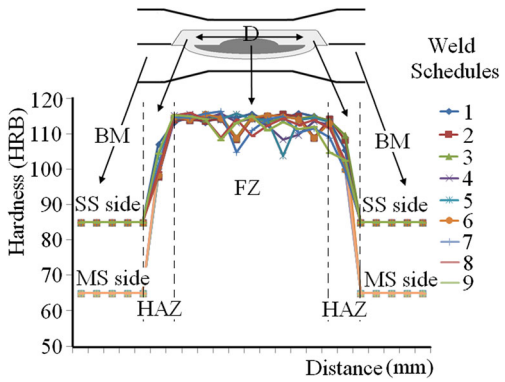

Fig. 24 Hardness of mixed steel

(i) The mild and dissimilar steels' micrographs have shown the fusion, heat-affected, heat-extended, and base metal zones very clearly, but the stainless steel's heat-affected and heat-extended zones are not visible at microlevel zooming because of the narrowed regions.

(j) Metallurgical views have clearly shown that the heat imbalance has occurred in mixed weld joints due to different electrical resistivity and thermal conductivity rates.

Acknowledgments I would like to thank the Ministry of Science, Technology and Innovation, Malaysia (MOSTI) for their financial support during the experiment. This research is an extension of my post-doctoral research work at the University Malaya, Malaysia.

References

1. Aravinthan A, Nachimani C, (2011) Analysis of spot welds growth on mild and stainless steel (1 mm). Welding Journal, August: 143–147
2. Cha BW, Na SJ (2003) A study on the relationship between welding conditions and residual stress of resistance. J Manuf Syst 22:31–40
3. Amuda MOH, Mridha S (2009) Micro structural features of AISI 430 ferritic stainless steel weld produced under varying process parameters. Int J Mech Mater Eng 4(2):160–166
4. Jamasri MN, Ilman R, Soekrisno T (2011) Corrosion fatigue behavior of RSW dissimilar metal welds between carbon steel and austenitic stainless steel with different thickness. Procedia Eng 10:649–654
5. Bayraktar E, Moiron J, Kaplan D (2006) Effect of welding conditions on the formability characteristics of thin sheet steels: mechanical and metallurgical effects. J Mater Process Technol 175:20–26
6. Triyono A (2009) Comparative study of fatigue assessment methods with and without considering residual stress on resistance spot-welded unequal sheet thickness stainless steel. Int J Eng Technol 11:456–462
7. Marashi P, Pouranvari M, Amirabdollahian S, Abedi A, Goodarzi M, (2008) Microstructure and failure behavior of dissimilar resistance spot welds between low carbon galvanized and austenitic stainless steels. Materials Science and Engineering A: 175–180
8. Pouranvari M (2011) Analysis of fracture mode of galvanized low carbon steel resistance spot welds. Int J Multidiscip Sci Eng 2(6):66–72
9. Aravinthan A, Nachimani C (2011) Metallurgical study of spot weld growth on mild steel with 1 mm and 2 mm thicknesses. J Inst Eng Malaysia 72:36–42
10. Shamsul JB, Hisyam MM (2007) Study of spot welding of austenitic stainless steel type 304. J Appl Sci Res 3(11):1494–1499
11. Lee WS (2004) Deformation and failure response of 304L stainless steel SMAW joint under dynamic shear loading. Mater Sci Eng A 381:206–215
12. Darwish SM (2003) Weld bonding strengths and balances the stresses in spot welded dissimilar thickness joints. J Mater Process Technol 134:352–362
13. Darwish SM, Al-Samhan AM (2004) Peel and shear strength of spot-welded and weld-bonded dissimilar thickness joints. J Mater Process Technol 147:138–146
14. Kent P, Von M, Henning EN (2000) Comparison of peel bond and shear tensile test methods for needle punched geo synthetic clay liners. Geotext Geomembr 18:203–214

15. Khodabakhshi F, Kazeminezhad M, Kokabi AH (2011) Mechanical properties and microstructure of resistance spot welded severely deformed low carbon steel. Mater Sci Eng A 15:356–343
16. Dursun O, Zyurek Z (2008) An effect of weld current and weld atmosphere on the resistance spot weld ability of 304L austenitic stainless steel. Mater Des 29:597–603
17. Fukumoto S, Fujiwara K, Toji S, Yamamoto A (2008) Small-scale resistance spot welding of austenitic stainless steels. Mater Sci Eng A 492:243–249
18. Pouranvari M, Marashi SPH (2010) Key factors influencing mechanical performance of dual phase steel resistance spot welds. Sci Technol Weld Join 15:149–155
19. Gould JE, Khurana SP, Li T, (2006) Predictions of microstructures when welding automotive advanced high-strength steels. Welding Journal 86:111s–116s
20. Pilar DT, Oscar M, Manuel L (2011) Combined effect of resistance spot welding and post-welding sensitization on the degree of sensitization of AISI 304 stainless steel. Corros Sci 53:2670–2675